Inorganic Chemistry

Article

pubs.acs.org/IC

Structure and Emissive Properties of Heterobimetallic Ln–Au Coordination Polymers: Role of Tb and Eu in Non-aurophilic $[^nBu_4N]_2[Ln(NO_3)_4Au(CN)_2]$ versus Aurophilic $Ln[Au(CN)_2]_3\cdot 3H_2O/3D_2O$ Chains

John C. Ahern,[†] Ryan J. Roberts,[‡] Philip Follansbee,[†] Jeffrey McLaughlin,[†] Daniel B. Leznoff,*[,‡] and Howard H. Patterson*[,†]

[†]Department of Chemistry, University of Maine, Orono, Maine 04469, United States

[‡]Department of Chemistry, Simon Fraser University, Burnaby, British Columbia V5A 1S6, Canada

Supporting Information

ABSTRACT: This investigation is focused on comparing photophysical properties between two series of lanthanide-dicyanoaurate coordination polymers that contain and lack aurophilic interactions, respectively. Luminescence and crystallographic studies have been carried out on five different coordination polymer chain frameworks: the non-aurophilic $[^nBu_4N]_2[Ln_xGd_{1-x}(NO_3)_4Au(CN)_2]$ (Ln = Eu, Tb; x = 0.01, 0.02, 0.04, 0.08) and $[^nBu_4N]_2[Eu_xTb_{1-x}(NO_3)_4Au(CN)_2]$ (x = 0.25, 0.5, 0.75), as well as the analogous solid-solutions of aurophilic $Ln_xGd_{1-x}[Au(CN)_2]_3\cdot 3H_2O$ and $Eu_xTb_{1-x}[Au(CN)_2]_3\cdot 3H_2O$. The single-crystal structures of $M[Au(CN)_2]_3\cdot 3H_2O$ (M = Eu, Gd) are also reported for comparison. In the aurophilic frameworks the close proximity of gold(I) centers on neighboring chains allows for Au–Au interactions to take place that facilitate energy transfer between lanthanides. Terbium- and europium-doped aurophilic frameworks show energy transfer between one of the lanthanide ions and dicyanoaurate centers as observed via luminescence measurements. In the non-aurophilic frameworks the $[^nBu_4N]$ cations separate the Au–Au chains, thereby preventing interaction between them, and preventing energy transfer. By preparing the aurophilic $Eu_xTb_{1-x}[Au(CN)_2]_3\cdot 3D_2O$ frameworks, it was shown that the O–H vibrational energy in the hydrated (aurophilic) samples can partially quench the Ln signal.

INTRODUCTION

Certain lanthanide ions are known to be highly emissive and can be incorporated into multifunctional luminescent materials which can reflect the magnetic, optical, and electronic properties of the parent lanthanide ions.[1−4] In such luminescent materials, the pairing of emissive lanthanide ions—which have sharp emission lines and long lifetimes—with potentially emissive transition metals is of great interest, in particular since the transition metal ions are often utilized to sensitize lanthanide-based emissions via energy transfer. The energy transfer is made possible by an overlap between the emission energy of the transition-metal activator and the excitation energy of the sensitized lanthanide.[5−7] This overlap allows single incident photons to interact with each component (transition-metal and lanthanide) to produce a single photon emission. Transition metals are generally superior to traditional organic sensitizers since they are closer in energy to the Ln^{3+} acceptors and have higher quantum yields.[8−13] In addition, incorporating a heavier transition metal, which has high spin–orbit-coupling like the lanthanides, can allow for more intersystem crossing which in turn allows for an increased quantum yield.[14]

With these points in mind, we have targeted a series of lanthanide/gold-containing coordination polymer materials.[15] It is well-known that Au(I), along with other d^{10} metal-containing systems can be exceedingly emissive, especially in cases where gold–gold, aurophilic, interactions[16,17] are present, and the luminescence can be used in photonic devices.[18−20] With the understanding of structure and properties generated through the design of specific frameworks, coordination polymers with particular shapes and topologies can be accessed, targeting applications such as light conversion, lasers, optical fiber coatings, LEDs, optical displays, and luminescent devices.[3,4,21−25] The intent of this study is to achieve a better understanding of the properties of lanthanide–gold coordination polymers through the investigation of energy transfer.

The emissive properties of the 3-D Kagomé-type $Ln[Au(CN)_2]_3\cdot 3H_2O$ framework, which contains chains of aurophilic interactions throughout the superstructure, has been extensively examined for several different Ln ions.[7,26−38] In many cases the use of two emissive elements (Au and Ln) allows for energy transfer between the two in the form of sensitization or quenching.[7,39] We also recently reported the use of an analogous non-aurophilic framework: $[^nBu_4N]_2[Ln(NO_3)_4Au(CN)_2]$ (Ln = Nd, Eu, Gd, Tb) that does not have inter- or

Received: April 15, 2014
Published: June 26, 2014

   dx.doi.org/10.1021/ic500890r | Inorg. Chem. 2014, 53, 7571−7579

intrachain aurophilic interactions. The lack of efficient energy transfer between the gold and lanthanide in this framework allowed for two distinct chromophores to be observed.[15]

Energy transfer is also possible between two or more lanthanides, such as terbium to europium, where both are present in the same material.[40] In such cases the $^5D_0$ level of Eu^{3+} is sensitized by the $^5D_4$ level of the Tb^{3+} ion.[40] In an effort to examine the effect of mixing lanthanide chromophores with Au-containing materials both with and without aurophilic interactions and to explore whether color-tuning might be possible by controlling the mixture ratios of emitting centers, we targeted the synthesis of mixed lanthanide/Au aurophilic frameworks $Ln_xLn'_{1-x}[Au(CN)_2]_3{\cdot}3H_2O$ and the non-aurophilic analogues $[^nBu_4N]_2[Ln_xLn'_{1-x}(NO_3)_4Au(CN)_2]$ where Ln or Ln′ = Gd, Eu or Tb; the deuterated $Eu_xTb_{1-x}[Au(CN)_2]_3{\cdot}3D_2O$ versions were also prepared in several cases to probe the role of O−H bonds in energy transfer. The excitation and emission spectra were examined as a function of Ln:Ln′ solid solution ratios for the aurophilic versus the non-aurophilic frameworks, thereby allowing differences in energy transitions to be correlated with structural data to form a more complete understanding of the photophysics of the different framework types.

EXPERIMENTAL SECTION

General Materials and Procedures. All materials were obtained from commercial sources and used as received unless otherwise indicated. Infrared spectra were recorded on a Thermo Nicolet Nexus 670 FTIR spectrometer equipped with Perkin-Elmer Spectrum One FT-IR spectrometer coupled with a Pike MIRacle attenuated total reflection (ATR) sampler. Microanalyses (C, H, N) were performed by Frank Haftbaradaran at Simon Fraser University on a Carlo Erba EA 1110 CHN elemental analyzer. Reflectance spectra were recorded with an Ocean Optics usb4000 spectrometer coupled to a fiber-optic probe. Halogen and helium arc lamps were used as light sources. Reflectance scans were run with an integration time of 4 ms, and 50 scans were averaged for each spectra.

Syntheses. The syntheses of the mixed lanthanide-containing materials below are based on modifications of literature procedures for the synthesis of $[^nBu_4N]_2[Gd(NO_3)_4Au(CN)_2]$[15] and $Gd[Au(CN)_2]_3{\cdot}3H_2O$.[27]

Synthesis of $[^nBu_4N]_2[Eu_xTb_{1-x}(NO_3)_4Au(CN)_2]$ (x = 0.25, 0.50, 0.75). A typical synthesis, using x = 0.50 as an example, is described. A solution of $[^nBu_4N][NO_3]$ (0.061 g, 0.2 mmol) and $[^nBu_4N][Au(CN)_2]{\cdot}1/2H_2O$ (0.100 g, 0.2 mmol) in 4 mL ethyl acetate (EtOAc) was added to a solution of $Eu(NO_3)_3{\cdot}6H_2O$ (43 mg, 0.1 mmol) and $Tb(NO_3)_3{\cdot}5H_2O$ (44 mg, 0.1 mmol) in 2 mL EtOAc. Colorless crystals were harvested by vacuum filtration after 1 day. Yield: 192 mg, 84.4%. Anal. Calcd for $C_{34}H_{72}N_8AuEu_{0.5}O_{12}Tb_{0.5}$: C 35.90%, H 6.38%, N 9.85%; found C 35.84%, H 6.27%, N 9.67. IR (ATR, cm^{-1}): 2958 (m), 2933 (m), 2874 (m), 2184 (ν_{CN}, m), 2151 (ν_{CN}, w), 1461 (s, br), 1315 (vs), 1152 (w), 1028 (m), 885 (w), 818 (w), 741 (m). For x = 0.25, Yield: 182 mg, 79.9%. For x = 0.75, Yield: 197 mg, 86.8%.

Synthesis of $Eu_xTb_{1-x}[Au(CN)_2]_3{\cdot}3H_2O$ (x = 0.25, 0.50, 0.75). A typical synthesis, using x = 0.50 as an example, is described. A solution of $K[Au(CN)_2]$ (173 mg, 0.6 mmol) in 1 mL of water was added to a solution of $Eu(NO_3)_3{\cdot}6H_2O$ (43 mg, 0.1 mmol) and $Tb(NO_3)_3{\cdot}5H_2O$ (44 mg, 0.1 mmol) in 2 mL of water. Pale-yellow (with intensity increasing corresponding to increasing Eu component) crystals were harvested by vacuum filtration after 1 day. Yield: 78 mg, 40.8%. Anal. Calcd for $C_6H_6N_6Au_3Eu_{0.5}O_3Tb_{0.5}$: C 7.53%, H 0.63%, N 8.79%; found C 7.38%, H 0.83%, N 8.41. IR (ATR, cm^{-1}): 3581 (m), 3525 (m), 2153 (ν_{CN}, s), 2114 (ν_{CN}, w), 1607 (m). For x = 0.25, Yield: 88 mg, 45.9% IR (ATR, cm^{-1}): 3589 (m), 3529 (m), 2153 (ν_{CN}, s), 2115 (ν_{CN}, w), 1606 (m). For x = 0.75, Yield: 91 mg, 47.7% IR (ATR, cm^{-1}): 3581 (m), 3525 (m), 2152 (ν_{CN}, s), 2114 (ν_{CN}, w), 1606 (m).

Synthesis of $Eu_xTb_{1-x}[Au(CN)_2]_3{\cdot}3D_2O$ (x = 0, 0.25, 0.50, 0.75, 1). Synthesis of the deuterated samples were carried out in an analogous fashion to $Eu_xTb_{1-x}[Au(CN)_2]_3{\cdot}3H_2O$, with the exception of being carried out in D_2O instead of H_2O. For x = 0, Yield: 86 mg, 44.5%. IR (ATR, cm^{-1}): 2675 (m), 2584 (m), 2154 (ν_{CN}, s), 2114 (ν_{CN}, w), 1188 (m). For x = 0.25, Yield: 103 mg, 53.4%. IR (ATR, cm^{-1}): 2672 (m), 2582 (m), 2153 (ν_{CN}, s), 2113 (ν_{CN}, w), 1188 (m). For x = 0.50, Yield: 84 mg, 43.6%. IR (ATR, cm^{-1}): 2672 (m), 2581 (m), 2152 (ν_{CN}, s), 2114 (ν_{CN}, w), 1188 (m). For x = 0.75, Yield: 120 mg, 62.4%. IR (ATR, cm^{-1}): 2670 (m), 2580 (m), 2152 (ν_{CN}, s), 2114 (ν_{CN}, w), 1189 (m). For x = 1; yield 130 mg, 67.8%. IR (ATR, cm^{-1}): 2669 (m), 2579 (m), 2152 (ν_{CN}, s), 2113 (ν_{CN}, w), 1189 (m).

Synthesis of $[^nBu_4N]_2[Eu_xGd_{1-x}(NO_3)_4Au(CN)_2]$ (x = 0.01, 0.02, 0.04, 0.08). A typical synthesis, using x = 0.08 as an example, is described. A 0.002 mol L^{-1} stock solution of $Eu(NO_3)_3{\cdot}6H_2O$ in ethyl acetate was prepared, and an aliquot (8.00 mL, 0.016 mmol) was added to $Gd(NO_3)_3{\cdot}6H_2O$ (83.1 mg, 0.184 mmol) and topped up to a total volume of 8 mL of ethyl acetate. To this, a 2 mL solution containing $[^nBu_4N][NO_3]$ (61 mg, 0.2 mmol) and $[^nBu_4N][Au(CN)_2]{\cdot}1/2H_2O$ (100 mg, 0.2 mmol) was added. Colorless crystals were obtained via vacuum filtration after 1 day. Yield: 190 mg, 83.4%. Anal. Calcd for $C_{34}H_{72}N_8AuEu_{0.08}Gd_{0.92}O_{12}$: C 35.86%, H 6.37%, N 9.84%; found C 35.80%, H 6.59%, N 9.72. IR (ATR, cm^{-1}): 2958 (m), 2933 (m), 2873 (m), 2185 (ν_{CN}, m), 2156 (ν_{CN}, m) 1461 (s, br), 1316 (vs), 1153 (w), 1028 (m), 884 (w), 818 (w), 742 (m). For x = 0.01, a 1.00 mL aliquot of 0.002 mol L^{-1} $Eu(NO_3)_3{\cdot}6H_2O$ stock solution was used with 89.4 mg (0.198 mmol) $Gd(NO_3)_3{\cdot}6H_2O$. Yield: 200 mg, 87.8%. IR (ATR, cm^{-1}): 2958 (m), 2934 (m), 2873 (m), 2185 (ν_{CN}, m), 2159 (ν_{CN}, w), 2147 (ν_{CN}, w), 1461 (s, br), 1316 (vs), 1153 (w), 1028 (m), 885 (w), 818 (w), 742 (m). For x = 0.02, a 2.00 mL aliquot of 0.002 mol L^{-1} $Eu(NO_3)_3{\cdot}6H_2O$ stock solution was used with 88.5 mg (0.196 mmol) $Gd(NO_3)_3{\cdot}6H_2O$. Yield: 212 mg, 93.0%. IR (ATR, cm^{-1}): 2958 (m), 2933 (m), 2874 (m), 2185 (ν_{CN}, m), 2159 (ν_{CN}, w), 2146 (ν_{CN}, w), 1461 (s, br), 1316 (vs), 1153 (w), 1028 (m), 884 (w), 818 (w), 742 (m). For x = 0.04, a 4.00 mL aliquot of 0.002 mol L^{-1} $Eu(NO_3)_3{\cdot}6H_2O$ stock solution was used with 86.7 mg (0.192 mmol) $Gd(NO_3)_3{\cdot}6H_2O$. Yield: 190 mg, 83.4%. IR (ATR, cm^{-1}): 2959 (m), 2934 (m), 2874 (m), 2185 (ν_{CN}, m), 2161 (ν_{CN}, w), 2146 (ν_{CN}, w), 1462 (s, br), 1315 (vs), 1153 (w), 1028 (m), 885 (w), 818 (w), 742 (m).

Synthesis of $[^nBu_4N]_2[Tb_xGd_{1-x}(NO_3)_4Au(CN)_2]$ (x = 0.01, 0.02, 0.04, 0.08). This synthesis was carried out in a reaction entirely analogous to that of $[^nBu_4N]_2[Eu_xGd_{1-x}(NO_3)_4Au(CN)_2]$. A typical synthesis, using x = 0.08 as an example, is described. A 0.002 mol L^{-1} stock solution of $Tb(NO_3)_3{\cdot}6H_2O$ in ethyl acetate was prepared, and an aliquot (8.00 mL, 0.016 mmol) was added to $Gd(NO_3)_3{\cdot}6H_2O$ (83.1 mg, 0.184 mmol) and topped up to a total volume of 8 mL of ethyl acetate. To this was added a 2 mL solution containing $[^nBu_4N][NO_3]$ (61 mg, 0.2 mmol) and $[^nBu_4N][Au(CN)_2]{\cdot}1/2H_2O$ (100 mg, 0.2 mmol). Colorless crystals were obtained via vacuum filtration after 1 day. Yield: 185 mg, 81.2%. For x = 0.01, a 1.00 mL aliquot of 0.002 mol L^{-1} $Tb(NO_3)_3{\cdot}5H_2O$ stock solution was used with 89.4 mg (0.198 mmol) $Gd(NO_3)_3{\cdot}6H_2O$. Yield: 197 mg, 86.5%. IR (ATR, cm^{-1}): 2959 (m), 2936 (m), 2874 (m), 2185 (ν_{CN}, m), 2146 (ν_{CN}, w), 1460 (s, br), 1315 (vs), 1153 (w), 1028 (m), 885 (w), 818 (w), 742 (m). For x = 0.02, a 2.00 mL aliquot of 0.002 mol L^{-1} $Tb(NO_3)_3{\cdot}5H_2O$ stock solution was used with 88.5 mg (0.196 mmol) $Gd(NO_3)_3{\cdot}6H_2O$. Yield: 192 mg, 84.3% IR (ATR, cm^{-1}): 2959 (m), 2932 (m), 2874 (m), 2185 (ν_{CN}, m), 2147 (ν_{CN}, w), 1461 (s, br), 1315 (vs), 1152 (w), 1028 (m), 884 (w), 818 (w), 742 (m). For x = 0.04, a 4.00 mL aliquot of 0.002 mol L^{-1} $Tb(NO_3)_3{\cdot}5H_2O$ stock solution was used with 86.7 mg (0.192 mmol) $Gd(NO_3)_3{\cdot}6H_2O$. Yield: 196 mg, 86.0%. IR (ATR, cm^{-1}): 2958 (m), 2933 (m), 2874 (m), 2185 (ν_{CN}, m), 2146 (ν_{CN}, w), 1461 (s, br), 1316 (vs), 1152 (w), 1029 (m), 884 (w), 818 (w), 742 (m).

Synthesis of $Eu_xGd_{1-x}[Au(CN)_2]_3{\cdot}3H_2O$ (x = 0.01, 0.02, 0.04, 0.08). A typical synthesis, using x = 0.08 as an example, is described. A 0.008 mol L^{-1} stock solution of $Eu(NO_3)_3{\cdot}6H_2O$ in water was prepared, and an appropriate aliquot (2.00 mL, 0.002 mmol) was added to $Gd(NO_3)_3{\cdot}6H_2O$ (83.1 mg, 0.184 mmol) and topped up to a

dx.doi.org/10.1021/ic500890r | Inorg. Chem. 2014, 53, 7571−7579

total volume of 2 mL of water. To this was added a 1 mL solution containing $K[Au(CN)_2]$ (173 mg, 0.6 mmol). Pale-yellow crystals were obtained via vacuum filtration after 1 day. Yield: 114 mg, 59.5%. Anal. Calcd for $C_6H_6N_6Au_3Eu_{0.08}Gd_{0.92}O_3$: C 7.52%, H 0.63%, N 8.77%; Found C 7.25%, H 0.69%, N 8.39. IR (ATR, cm^{-1}): 3581 (m), 3525 (m), 2153 (ν_{CN}, s), 2115 (ν_{CN}, w), 1607 (m). For x = 0.01, a 0.250 mL aliquot of 0.008 mol L^{-1} $Eu(NO_3)_3{\cdot}6H_2O$ stock solution was used with 89.4 mg (0.198 mmol) $Gd(NO_3)_3{\cdot}6H_2O$. Yield: 112 mg, 58.4%. IR (ATR, cm^{-1}): 3581 (m), 3530 (m), 2153 (ν_{CN}, s), 2113 (ν_{CN}, w), 1607 (m). For x = 0.02, a 0.500 mL aliquot of 0.008 mol L^{-1} $Eu(NO_3)_3{\cdot}6H_2O$ stock solution was used with 88.5 mg (0.196 mmol) $Gd(NO_3)_3{\cdot}6H_2O$. Yield: 124 mg, 64.7%. IR (ATR, cm^{-1}): 3581 (m), 3520 (m), 2153 (ν_{CN}, s), 2114 (ν_{CN}, w), 1607 (m). For x = 0.04, a 1.00 mL aliquot of 0.008 mol L^{-1} $Eu(NO_3)_3{\cdot}6H_2O$ stock solution was used with 86.7 mg (0.192 mmol) $Gd(NO_3)_3{\cdot}6H_2O$. Yield: 112 mg, 58.4%. IR (ATR, cm^{-1}): 3581 (m), 3523 (m), 2153 (ν_{CN}, s), 2114 (ν_{CN}, w), 1607 (m).

Synthesis of $Tb_xGd_{1-x}[Au(CN)_2]_3{\cdot}3H_2O$ (x = 0.01, 0.02, 0.04, 0.08). The synthesis was carried out in a reaction analogous to that of $Eu_xGd_{1-x}[Au(CN)_2]_3{\cdot}3H_2O$. A typical synthesis, using x = 0.08 as an example, is described. A 0.008 mol L^{-1} stock solution of $Tb(NO_3)_3{\cdot}5H_2O$ in water was prepared, and an appropriate aliquot (2.00 mL, 0.002 mmol) was added to $Gd(NO_3)_3{\cdot}6H_2O$ (83.1 mg, 0.184 mmol) and topped up to a total volume of 2 mL of water. To this was added a 1 mL solution containing $K[Au(CN)_2]$ (173 mg, 0.6 mmol). Colorless crystals were obtained via vacuum filtration after 1 day. Yield: 104 mg, 54.2%. Anal. Calcd for $C_6H_6N_6Au_3Gd_{0.92}Tb_{0.08}O_3$: C 7.52%, H 0.63%, N 8.77%; found C 7.34%, H 0.67%, N 8.38. IR (ATR, cm^{-1}): 3584 (m), 3529 (m), 2153 (ν_{CN}, s), 2115 (ν_{CN}, w), 1607 (m). For x = 0.01, a 0.250 mL aliquot of 0.008 mol L^{-1} $Tb(NO_3)_3{\cdot}5H_2O$ stock solution was used with 89.4 mg (0.198 mmol) $Gd(NO_3)_3{\cdot}6H_2O$. Yield: 119 mg, 62.0%. IR (ATR, cm^{-1}): 3584 (m), 3529 (m), 2153 (ν_{CN}, s), 2115 (ν_{CN}, w), 1607 (m). For x = 0.02, a 0.50 mL aliquot of 0.008 mol L^{-1} $Tb(NO_3)_3{\cdot}5H_2O$ stock solution was used with 88.5 mg (0.196 mmol) $Gd(NO_3)_3{\cdot}6H_2O$. Yield: 124 mg, 64.7%. IR (ATR, cm^{-1}): 3584 (m), 3529 (m), 2153 (ν_{CN}, s), 2115 (ν_{CN}, w), 1607 (m). For x = 0.04, a 1.000 mL aliquot of 0.008 mol L^{-1} $Tb(NO_3)_3{\cdot}5H_2O$ stock solution was used with 86.7 mg (0.196 mmol) $Gd(NO_3)_3{\cdot}6H_2O$. Yield: 116 mg, 60.5%. IR (ATR, cm^{-1}): 3584 (m), 3530 (m), 2153 (ν_{CN}, s), 2115 (ν_{CN}, w), 1607 (m).

X-ray Crystallography. Powder X-ray diffractograms of $[^nBu_4N]_2[Eu_{0.08}Gd_{0.92}(NO_3)_4Au(CN)_2]$, $[^nBu_4N]_2[Tb_{0.08}Gd_{0.92}(NO_3)_4Au(CN)_2]$, $Eu_{0.08}Gd_{0.92}[Au(CN)_2]_3{\cdot}3H_2O$, and $Tb_{0.08}Gd_{0.92}[Au(CN)_2]_3{\cdot}3H_2O$ were collected using a Bruker SMART APEX II equipped with a Incoatec IμS Cu Kα source (λ = 1.54056 Å). Samples were mounted on MiTeGen sample holders using paratone oil and were exposed as the phi axis was spinning (6 deg s^{-1}), for a period of 60 min. Diffractograms and the comparison with the simulated diffractograms (from single-crystal data) for the undoped-Gd-based systems are in Figures S1 and S2 in the SI.

Single crystals of $[^nBu_4N]_2[Eu_{0.5}Tb_{0.5}(NO_3)_4Au(CN)_2]$, $Eu_{0.5}Tb_{0.5}[Au(CN)_2]_3{\cdot}3H_2O$ $Eu[Au(CN)_2]_3{\cdot}3H_2O$, and $Gd[Au(CN)_2]_3{\cdot}3H_2O$ were mounted on a MiTeGen sample holder using paratone oil, and the data were collected at room temperature on a Bruker SMART APEX II diffractometer, and the data were processed with the Bruker APEX II software suite. The structures were solved with SIR92. Subsequent refinements were performed using CRYSTALS.[41] The coordinates and anisotropic displacement parameters for the non-hydrogen atoms were refined. Hydrogen atoms were placed in geometrically calculated positions and refined using a riding model. For $[^nBu_4N]_2[Eu_{0.5}Tb_{0.5}(NO_3)_4Au(CN)_2]$ the hydrogen atom isotropic thermal parameters were constrained. The lanthanide center was modeled with a 50% Eu 50% Tb occupancy disorder which was found to correspond to the combination which resulted in the lowest R value. It is inferred that this represents a random arrangement of Eu and Tb atoms in this position. The crystal was found to be a racemic twin and was modeled accordingly. The final refinement was conducted using the observed data ($I_o \geq 2.5\sigma(I_o)$). Diagrams were prepared using ORTEP-3[42] and POV-RAY.[43]

Luminescence Experiments. Steady-state photoluminescence spectra were collected with a model Quantamaster-1046 photoluminescence spectrometer from Photon Technology International. This instrument uses a 75-W xenon arc lamp along with two excitation monochromators and one emission monochromator to tune the bandwidth of light striking the sample and detector, respectively. Light intensity was measured using a photomultiplier tube. Low-temperature scans were run on the same system coupled to a Janis ST-100 optical cryostat. Liquid nitrogen was used as a coolant. Each sample was independently mounted on a copper holder using cry-con grease, a copper-dust, high-vacuum grease that is nonemissive within the range under examination. The spectra were run as collected sequential emission scans to form a 3-D matrix with excitation as the x axis, emission on the y axis, and intensity on the z axis. The wavelength of the exciting light was run from low to high wavelength at increments of 3 nm between 200 and 500 nm to avoid photobleaching, oxidation, or other forms of degradation. Luminescence lifetime measurements were collected by exciting crystals using a 300 nm source from an Opotek 355 II Tunable laser. The emission was collected at 540 nm using a Jobin Yvon Ramanor system, and the lifetime was read with a LeCroy oscilloscope, collecting data every 10 ns for 50 μs per sweep, averaging 1000 sweeps per sample. The 300 nm excitation and 540 nm emission wavelengths were chosen since the lanthanides can be excited and emitted at those chosen wavelengths.

RESULTS AND DISCUSSION

Syntheses. To explore the color tuning potential of the non-aurophilic $[^nBu_4N]_2[Ln(NO_3)_4Au(CN)_2]$ system (in which the Ln and Au chromophores are known to be independently observable),[15] the bimetallic lanthanide solid-solutions $[^nBu_4N]_2[Eu_xTb_{1-x}(NO_3)_4Au(CN)_2]$ with x = 0.25, 0.50, 0.75 were synthesized and characterized. To monitor the effect of concentration of the emitting unit (Tb or Eu) on the overall luminescence, the $[^nBu_4N]_2[Ln_xGd_{1-x}(NO_3)_4Au(CN)_2]$ system (Ln = Eu, Tb; x = 0.01, 0.02, 0.04, 0.08), where the Gd-center is nonemissive, was also synthesized and characterized.

For materials with values of $x \geq 0.25$ an ethyl acetate solution containing one equivalent of $[^nBu_4N][Au(CN)_2]{\cdot}1/2H_2O$ and $[^nBu_4N][NO_3]$ was added to an ethyl acetate solution of the appropriate mixture of $Ln(NO_3)_3{\cdot}nH_2O$ salts. For materials with values of $x \leq 0.08$ standard solutions of the minor $Ln(NO_3)_3{\cdot}nH_2O$ component (Ln = Eu, Tb) in ethyl acetate were made, and appropriate aliquots were added to solutions containing the principal component, $Gd(NO_3)_3{\cdot}6H_2O$. Both methods yielded crystals of the respective mixed lanthanide $[^nBu_4N]_2[Ln'_xLn_{1-x}(NO_3)_4Au(CN)_2]$ in good yields.

In order to examine the energy transfer properties of mixing Eu/Tb ions in an aurophilic framework, the solid-solutions of $Eu_xTb_{1-x}[Au(CN)_2]_3{\cdot}3H_2O$ (x = 0.25, 0.50, 0.75) were synthesized and characterized. In addition to this, deuterated analogues of these systems were prepared to determine the impact of O−H stretching modes on the resulting luminescence. To monitor the effect of concentration of the emitting unit on the overall luminescence of this mixed Eu/Tb system, the mixed lanthanide $Ln_xGd_{1-x}[Au(CN)_2]_3{\cdot}3H_2O$ (Ln = Eu, Tb; x = 0.01, 0.02, 0.04, 0.08) systems were also synthesized and characterized. As for the non-aurophilic synthetic methodology, for materials with values of $x \geq 0.25$ an aqueous solution of $K[Au(CN)_2]$ was added to an aqueous solution containing the appropriate ratio of $Ln(NO_3)_3{\cdot}nH_2O$ salts, while for materials with values of $x \leq 0.08$ stock solutions of the minor component were used. Both methods yielded crystals of $Ln'_xLn_{1-x}[Au(CN)_2]_3{\cdot}3H_2O$.

dx.doi.org/10.1021/ic500890r | Inorg. Chem. 2014, 53, 7571−7579

Structure of $[^nBu_4N]_2[Ln'_xLn_{1-x}(NO_3)_4Au(CN)_2]$ (Ln = Eu, Tb, Gd). A representative single-crystal structure for Ln′ = Eu, Ln = Tb, x = 0.50 was obtained. The structure of $[^nBu_4N]_2[Ln'_xLn_{1-x}(NO_3)_4Au(CN)_2]$, which is isostructural to the parent $[^nBu_4N]_2[Ln(NO_3)_4Au(CN)_2]$ as previously described,[15] consists of a one dimensional (1-D) zigzag coordination polymer with 10-coordinate lanthanide ions located in the vertices of the zigzag chain coordinated to four bidentate nitrate ligands and two nitriles from $[Au(CN)_2]^-$ groups (Figure 1). The dicyanoaurate units are separated in space such that no aurophilic bonding occurs, either intra- or interchain, the shortest Au−Au distance being ≈6.3 Å.[15] The lanthanides in the chain are likely randomly spaced throughout.

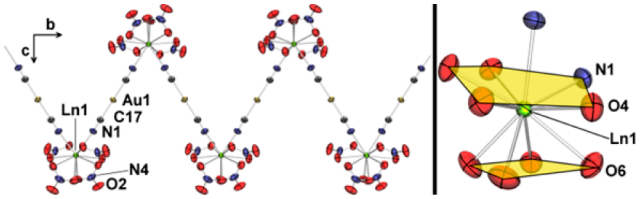

Figure 1. (Left) One-dimensional zigzag chain structure of $[^nBu_4N]_2[Ln(NO_3)_4Au(CN)_2]$. The two $[^nBu_4N]^+$ cations, which have been omitted for clarity, lie above and below the lanthanide center, and in between the lanthanides in the plane of the zigzag motif, respectively. (Right) Sphenocoronal coordination environment of the lanthanide center. Au, yellow; O, red; C, gray; N, blue. Ln, green.[15]

The coordination geometry is best described as a sphenocoronal structure, in which the vertices of the sphenocorona can be described as a square face opposed to a capped pentagonal face. The bottom square is composed of four oxygens originating from nitrates, the pentagon is composed of four nitrate oxygens and one dicyanoaurate nitrogen, and the pentagon is capped by a dicyanoaurate nitrogen (Figure 1, right).

Representative powder X-ray diffractograms of $[^nBu_4N]_2[Ln'_xLn_{1-x}(NO_3)_4Au(CN)_2]$ Ln′ = Eu, Tb, Ln = Gd; x = 0.08 (Figure S1 in the SI) indicate that the bulk solid-solution sample is isomorphous to the parent species $[^nBu_4N]_2[Ln(NO_3)_4Au(CN)_2]$.[15]

Structure of $Ln'_xLn_{1-x}[Au(CN)_2]_3{\cdot}3H_2O$. The structure of $Ln'_xLn_{1-x}[Au(CN)_2]_3{\cdot}3H_2O$, and the hereto uncharacterized $Eu[Au(CN)_2]_3{\cdot}3H_2O$, which are isostructural to the parent $Ln[Au(CN)_2]_3{\cdot}3H_2O$ series,[35,37] display a 9-coordinate lanthanide center with a tricapped trigonal prismatic geometry. The analogous $Gd[Au(CN)_2]_3{\cdot}3H_2O$ system is also reported, for which crystal structure data was previously reported but was interpreted in the wrong space group;[27,44] it is also in fact isostructural. Six $[Au(CN)_2]^-$ nitrile donors occupy the trigonal prismatic positions, and three H_2O units occupy the capped positions (Figure 2, right). This results in an interpenetrated 3-D coordination polymer. The Au atoms form layers with short Au−Au contacts of ≈3.3 Å.

Powder X-ray diffractograms of $Ln'_xLn_{1-x}[Au(CN)_2]_3{\cdot}3H_2O$ Ln′ = Eu, Tb, Ln = Gd; x = 0.08 (Figure S2 in the SI) indicate that the bulk solid-solution sample is isomorphous to the parent species $Ln'_xLn_{1-x}[Au(CN)_2]_3{\cdot}3H_2O$ (see Table 1).

Luminescence. Luminescence experiments were conducted to compare energy transfer pathways in aurophilic versus non-aurophilic Ln/Au networks and to investigate the effect of Ln dopant identity and concentration thereon. The emission spectra were used to determine how the aurophilic interactions affect the lanthanide emissions, while the excitation spectra were used to determine if energy transfer is occurring between any of the potentially emissive units. Indeed, there are differences; Figure 3 highlights the qualitative emission colors of the Eu/Tb mixtures as a function of Eu:Tb ratio and framework type. Each of these factors will be independently examined below.

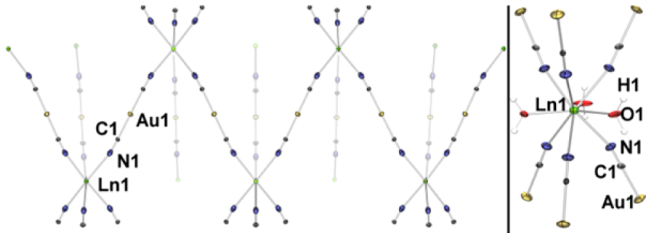

Figure 2. (Left) Three dimensional coordination polymer of $Ln[Au(CN)_2]_3{\cdot}3H_2O$ with extraplanar M−N−C-Au chains de-emphasized. H_2O molecules omitted for clarity. (Right) Coordination environment of the lanthanide center displaying a nine-coordinate tricapped trigonal prismatic structure.

The impact on the emission spectrum of doping Tb^{3+} into the non-aurophilic $[^nBu_4N]_2[Gd(NO_3)_4Au(CN)_2]$ framework at the 1, 2, 4, and 8% levels is shown in Figure 4. The peak around 430 nm corresponds to a known $Au(CN)_2^-$ MLCT emission.[26] The increased intensity of the 480, 540, and 625 nm peaks corresponds with the direct excitation of the increasingly concentrated terbium. Terbium peaks are observed in the 4% and 8% Tb-doped samples and may be present in the 1 and 2% cases as well, but the $Au(CN)_2^-$ MLCT emissions are prominent enough to make it hard to discriminate other peaks. The excitation peaks at 320, 374, 380, and 490 nm correspond with direct excitation of terbium. The excitation and emission assignments are in agreement with previously published works.[15,30] Efficient energy transfer from the donor $Au(CN)_2^-$ to the terbium acceptor should induce quenching of the $Au(CN)_2^-$ MLCT peak. Since this does not occur in $[^nBu_4N]_2[Tb(NO_3)_4Au(CN)_2]$ there is little to no energy transfer between the dicyanoaurate and the lanthanide metal centers. The results show little difference from previously reported emissions for $[^nBu_4N]_2[Tb(NO_3)_4Au(CN)_2]$ (i.e., with 100% Tb in the lanthanide site).[15] Gd has no transitions in the experimental excitation and emission window and, as such, does not have any effect on the observed luminescence.

Figure 5 shows the aurophilic $Gd[Au(CN)_2]_3{\cdot}3H_2O$ framework with different amounts of terbium. Peaks around 540 and 580 nm are observed for the 8% terbium-doped sample, which corresponds with energy transfer between the gold and the emissive Tb^{3+}. Unlike the spectra for the non-aurophilic samples in Figure 4, there are no sharp peaks in Figure 5 between 320 and 380 nm, which would be associated with the direct excitation of terbium. Thus, we hypothesize that the observed terbium-based emissions are made possible by absorption of energy by the gold and its subsequent transfer to the terbium. The orientation of Au−Au chains from the $Gd[Au(CN)_2]_3{\cdot}3H_2O$ allows for an aurophilic network to form that allows for energy transfer from the gold to terbium. There is little difference in luminescence spectra with variation in terbium loading below 8%, at which point the 430 nm $Au(CN)_2^-$ MLCT peak red-shifts to 435 nm because of the crystal field effect of the added Tb^{3+} ions.[45,46] Table 2 gives the specific excitation and emission wavelengths corresponding

dx.doi.org/10.1021/ic500890r | Inorg. Chem. 2014, 53, 7571−7579

Table 1. Crystallographic Data Table for $[^nBu_4N]_2[Eu_xTb_{1-x}(NO_3)_4Au(CN)_2]$, $Eu_{0.5}Tb_{0.5}[Au(CN)_2]_3{\cdot}3H_2O$, and $Ln[Au(CN)_2]_3{\cdot}3H_2O$ (Ln = Eu, Gd)

cmpd abbreviation	$[^nBu_4N]_2[Eu_{0.5}Tb_{0.5}(NO_3)_4Au(CN)_2]$	$Eu_{0.5}Tb_{0.5}[Au(CN)_2]_3{\cdot}3H_2O$	$Eu[Au(CN)_2]_3{\cdot}3H_2O$	$Gd[Au(CN)_2]_3{\cdot}3H_2O$
empirical formula	$C_{34}H_{72}N_8AuEu_{0.50}O_{12}Tb_{0.50}$	$C_6H_6N_6Au_3Eu_{0.50}O_3Tb_{0.50}$	$C_6H_6N_6Au_3EuO_3$	$C_6H_6N_6Au_3GdO_3$
formula weight ($g{\cdot}mol^{-1}$)	1137.40	956.50	953.01	952.28
crystal system	orthorhombic	hexagonal	hexagonal	hexagonal
space group	$I2_12_12_1$	$P6_3/mcm$	$P6_3/mcm$	$P6_3/mcm$
a (Å)	12.0199(3)	6.63180(10)	6.63800(10)	6.6317(9)
b (Å)	12.0211(3)	6.63180(10)	6.63800(10)	6.6317(9)
c (Å)	34.9690(10)	18.2231(4)	18.2725(3)	18.237(3)
α (deg)	90	90	90	90
β (deg)	90	90	90	90
γ (deg)	90	120	120	120
V (Å^3)	5052.8(2)	694.09(2)	697.273(19)	694.62(16)
Z	4	2	2	2
T (K)	293	293	293	293
ρ_{calcd} ($g{\cdot}cm^{-3}$)	1.495	4.576	4.539	4.536
μ (mm^{-1})	4.266	36.361	35.908	36.165
reflections $[I_o \geq 2.50\sigma(I_o)]$	6979	380	623	358
R, R_w $[I_o \geq 2.50\sigma(I_o)]$	0.0223, 0.0205	0.0266, 0.0332	0.0372, 0.0103	0.0138, 0.0112
goodness of fit	1.0772	0.8978	1.0782	1.0456

Figure 3. (Top) Photoluminescence of $[^nBu_4N]_2[Eu_xTb_{1-x}(NO_3)_4Au(CN)_2]$ using a long wavelength UV-lamp excitation source at room temperature; from left to right x = 1, 0.75, 0.50, 0.25, 0, illustrating color tuning ability. (Bottom) Photoluminescence of $Eu_xTb_{1-x}[Au(CN)_2]_3{\cdot}3H_2O$ using a long wavelength UV-lamp excitation source at 77 K; from left to right x = 0, 0.25, 0.50, 0.75, 1, illustrating the energy transfer resulting in only europium-based emission.

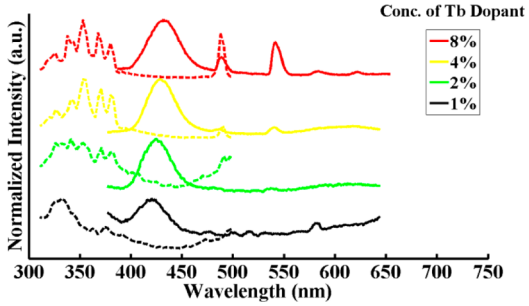

Figure 4. Excitation (dashed) and emission (solid) scans for the non-aurophilic $[^nBu_4N]_2[Tb_xGd_{1-x}(NO_3)_4Au(CN)_2]$ crystals with varying amounts of terbium (x = 0.08, 0.04, 0.02, 0.01) doped in them. The excitation used was 353 nm, and the emission used for the excitation scans was 540 nm to highlight the role of Tb and determine if energy transfer occurs. Resolution is 1 nm for the emissions and 3 nm for the excitations. Scans were performed at 77 K.

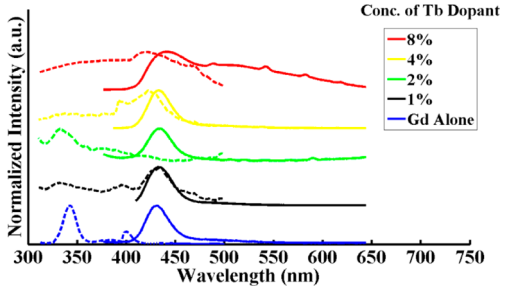

Figure 5. Excitation (dashed) and emission (solid) scans given an excitation of 353 nm and emission of 540 nm at 77 K for the aurophilic $Tb_xGd_{1-x}[Au(CN)_2]_3{\cdot}3H_2O$ crystals with varying amounts of terbium (x = 0.08, 0.04, 0.02, 0.01, 0) doped in them. Resolution is 1 nm for the emissions and 3 nm for the excitations.

with each type of transition associated with peaks in Figures 4 and 5.

Thus, in the non-aurophilic $[^nBu_4N]_2[Tb_xGd_{1-x}(NO_3)_4Au(CN)_2]$ system, increasing the Tb^{3+}-doping yields an increase in the Tb^{3+}-emission with no impact on the $Au(CN)_2^-$ MLCT band. However, in the aurophilic system some energy transfer

dx.doi.org/10.1021/ic500890r | Inorg. Chem. 2014, 53, 7571−7579

Table 2. Peak Assignments for Figures 4 and 5

excitation (nm)	emission (nm)	assignment
353	430	MLCT: Au−$(CN)_2^-$
340	474	MLCT: Au−$(CN)_2^-$
340, 420−430	540, 580	d-f (Au^+−Tb^{3+}) in Figure 5
320, 374, 380 490	540, 580	Tb^{3+} in Figure 4

from the Au-based emission to Tb^{3+} lines is observed as evidenced by a quenching of the Au-based emissions, although both emitting moieties are still independently observable at these low dopings.

Figure 6 shows the impact of doping Eu^{3+} into the non-aurophilic $[^nBu_4N]_2[Eu_xGd_{1-x}(NO_3)_4Au(CN)_2]$ framework.

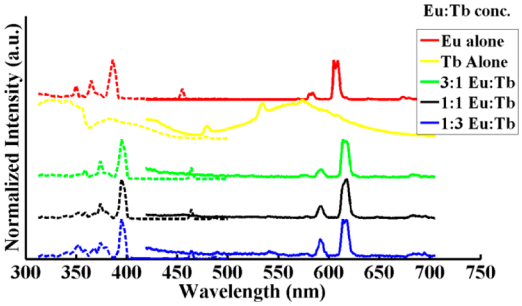

Figure 6. Excitation (dashed) and emission (solid) scans at 77 K given an excitation of 398 nm and emission of 589 nm for the non-aurophilic $[^nBu_4N]_2[Eu_xGd_{1-x}(NO_3)_4Au(CN)_2]$ crystals with varying amounts (x = 0.08, 0.04, 0.02, 0.01) of Eu^{3+}. Resolution is 1 nm for the emissions and 3 nm for the excitations.

Unlike for the terbium-doped system (Figure 4), there are far fewer peaks in the excitation spectra for the europium-doped system (Figure 6). The broad Au-based emission peaks around 435 nm represent the same transition as the 430 nm in the Tb-based system. The intensity of the Eu peaks increase with greater Eu loading relative to the Au-based emissions; however, it is not a result of energy transfer. Direct excitation of Eu^{3+} is differentiated from Au−Eu^{3+} energy transfer by the excitation spectra. Eu^{3+} can be directly excited at energies of 385, 460, 480, and 495 nm which induce emission peaks around 590 and 690 nm.[38] The expected electric dipole D_0-F_2 emission of Eu^{3+} at 615 nm is not present, yet there are bands associated with Eu^{3+} at 590 and 690 nm. This is likely because the symmetry of the Eu is virtually zero so the electric dipole emission is not favored.

Luminescence scans were also run on the aurophilic $Eu_xGd_{1-x}[Au(CN)_2]_3{\cdot}3H_2O$ framework with different loadings (x = 0.01, 0.02, 0.04, 0.08) of the Eu^{3+} dopant (Figure S3 in the SI). As in the non-aurophilic case (Figure 6), the Au-based emission peak around 435 nm decreases in intensity with greater Eu loading. This decrease is a sign of quenching of the $Au(CN)_2^-$ MLCT. The present association of the 590 nm peak with Au−Eu^{3+} energy transfer is supported by a previous study on europium-doped dicyanoaurate systems without gadolinium.[47] Table 3 gives the excitation and emission wavelengths corresponding to each type of charge transfer observed for the Eu-doped aurophilic and non-aurophilic frameworks.

Thus, europium-doping into either type of framework induces quenching of the $Au(CN)_2^-$ MLCT bands which results in a limited number of peaks in the excitation spectra and almost no peaks in the emission spectra except for the Eu^{3+}

Table 3. Peak Assignments for Figures 6 and S3 (in the SI)

excitation (nm)	emission (nm)	assignment
353	435	MLCT: ($Au-(CN)_2^-$)
385, 460, 480, 495	590	Eu^{3+} in Figures 6 and S3 (in the SI)

bands at 590 and 690 nm. As with the Tb^{3+}-doped systems, energy transfer is only observed for the aurophilic $Ln_xGd_{1-x}[Au(CN)_2]_3{\cdot}3H_2O$ framework because it is the only one that allows for interaction between neighboring Au−Au chains.

Figure 7 shows the aurophilic $Eu_xTb_{1-x}[Au(CN)_2]_3{\cdot}3H_2O$ framework with different stoichiometric ratios (x = 0, 0.25, 0.5,

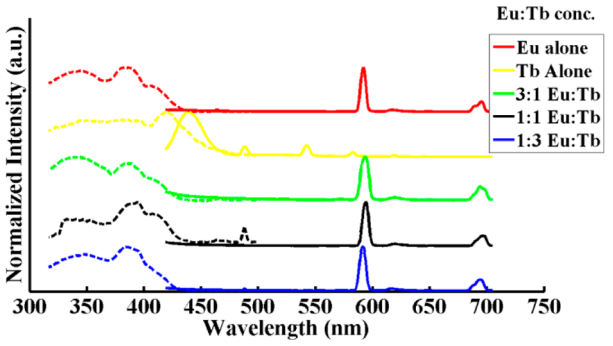

Figure 7. Excitation (dashed) and emission (solid) scans at 77 K given an excitation of 389 nm and emission of 589 nm of aurophilic $Eu_xTb_{1-x}[Au(CN)_2]_3{\cdot}3H_2O$ crystals with varying amounts (x = 1, 0, 0.75, 0.5, 0.25) of Eu:Tb. Resolution is 1 nm.

0.75, 1) of europium and terbium. Only the pure Tb-containing sample exhibits strong Tb-based emissions, with the peaks at 480, 541, and 575 nm. The other formulations lack such emission peaks, indicating that Eu is an effective quencher of terbium emissions. Given excitations of 400 and 410 nm, the aurophilic $Eu_xTb_{1-x}[Au(CN)_2]_3{\cdot}3H_2O$ samples produce an emission at 590 nm corresponding with a Tb−Eu energy transfer, as can be seen in Figure 7. The peaks around 690 nm are from direct excitation of Eu^{3+} which does occur simultaneously with energy transfer from terbium to europium. The energy transfer emissions seen at 590 nm are made possible by an excitation at 400 nm for the gold−europium energy transfer emission and an excitation of 410 nm for the Tb^{3+}−Eu^{3+} energy transfer emission. These assignments are in agreement with previously published results.[15,29,33,39,47] Luminescence scans were also run on a series of $Eu_xTb_{1-x}[Au(CN)_2]_3{\cdot}3D_2O$ (x = 0, 0.25, 0.5, 0.75, 1; Figure S4 in the SI). The ratio between the higher-energy 590 nm peak and the lower-energy peaks (especially 690 nm) is smaller for the H_2O samples versus the ratio for the D_2O samples. This is likely because the O−H vibrations from water are quenching some of the low-energy Ln emissions. On the basis of similar studies involving quenching of lanthanide emissions, the likely mechanism is dipole−dipole energy transfer from the electronically excited lanthanide ions to the isoenergetic O-H vibrational centers.[48]

Table 4 below gives the excitation and emission wavelengths associated with specific types of charge and energy transfer observed in Figures 7 and 8.

On the other hand, there is little to no energy transfer between the gold and lanthanides or between the two

dx.doi.org/10.1021/ic500890r | Inorg. Chem. 2014, 53, 7571−7579

Table 4. Peak Assignments for Figures 7, 8, and S4 in the SI

excitation (nm)	emission (nm)	assignment
320	540	Tb^{3+} in Figure 8
353	435	MLCT: $(Au-(CN)_2^-)$
340	474	MLCT: $(Au-(CN)_2^-)$
344, 368, 374	540	d-f: (Au^+-Tb^{3+})
400, 410	590	f-f: $(Tb^{3+}-Eu^{3+})$ in Figure 7
385, 460	590, 610, 618	Eu^{3+} in Figure 8
400	610, 618	d-f: $(Au^+$-Eu^{3+} S4 (in the SI)

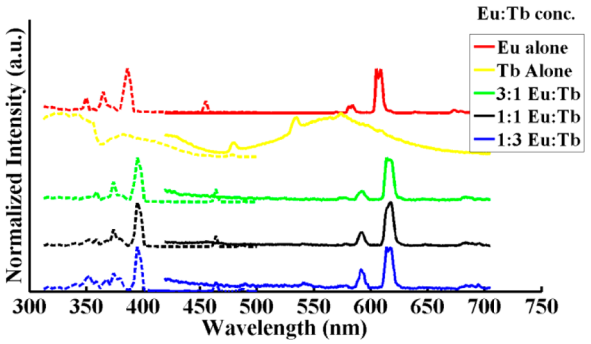

Figure 8. Excitation (dashed) and emission (solid) scans at 77 K given an excitation of 389 nm and emission of 589 nm of non-aurophilic $[^nBu_4N]_2[Eu_xTb_{1-x}(NO_3)_4Au(CN)_2]$ crystals with varying amounts (x = 1, 0, 0.75, 0.5, 0.25) of Eu:Tb. Resolution is 1 nm.

lanthanide ions in the non-aurophilic $[^nBu_4N]_2[Eu_xTb_{1-x}(NO_3)_4Au(CN)_2]$ framework (x = 0, 0.25, 0.5, 0.75, 1) (Figure 8). The lack of interaction allows for distinct Ln emissions to be observed. In the mixed Eu:Tb aurophilic samples only the europium emits since it quenches the terbium signal. There are peaks around 590 nm much like in Figure 7. However, unlike in Figure 7 these peaks are the result of direct excitation of the europium. For the non-aurophilic case emission was more pronounced at 618 nm than at 590 nm. This is a marked difference from the non-aurophilic system with just europium in it. When both Eu and Tb are present the lower energy (618 nm), emission is more pronounced than the 590 nm emission because the small energy difference between the Eu^{3+}- and Tb^{3+}-emitting states allows for the low-energy pathway to be favored. The claim for direct excitation versus energy transfer is supported by the fact there are peaks in the excitation spectra indicating each lanthanide and metal is excited individually (broad excitations from 320 to 340 nm for Tb^{3+} and 385 and 460 nm for Eu^{3+}). These assignments are in agreement with those previously published in the literature.[15] Having two distinct chromophores (see Figure 8) could allow one to tune the emissions based on excitation wavelength and stoichiometric ratio. Once again the wide terbium emissions seen in the terbium alone case are quenched by the europium even without energy transfer through aurophilic interactions. When these samples are subjected to a broader excitation band, distinct, concentration-dependent emissions are reported like those seen from the samples in the top half of Figure 3. The colors of Figure 3 are the sum of emission spectra at each wavelength of the exciting bandwidth. Also, once again spectra for non-aurophilic systems can be differentiated from aurophilic ones by the presence of excitation peaks, indicating direct excitation of a lanthanide followed by emission from that same lanthanide.

Lifetime Measurements. Luminescence lifetime measurements were conducted on crystal samples of the various doped frameworks. Samples were excited at 300 nm with a UV tunable laser, and emissions were observed at 541 nm for terbium-doped, 590 nm for europium-doped, and 430 nm for systems without any terbium or europium. An excitation of 300 nm was chosen since the laser pulses well at that wavelength and each sample can emit given that excitation. The emission wavelengths were chosen on the basis of the emission maxima common to each class of compound studied. Comparisons in lifetimes were made on the basis of two factors: (1) dopant level of a given framework and (2) type of framework. Tables 5 and 6 highlight the differences between non-aurophilic and aurophilic frameworks, respectively. Given the same dopant level the lifetimes are shorter for the aurophilic samples. The shorter lifetimes among the aurophilic cases can be explained by the increase in energy transfer between the dicyanoaurate units and the lanthanide ions in the aurophilic frameworks. Data in both tables show that the lifetimes decrease with increasing terbium dopant level, consistent with the fact that terbium centers facilitate energy transfer.

Table 5. Luminescence Lifetimes for the Non-aurophilic $[^nBu_4N]_2[Tb_xGd_{1-x}(NO_3)_4Au(CN)_2]$ Crystals with Terbium Dopant; Lifetimes Were Observed at 541 nm

Tb dopant level (%)	τ_1 (μs)	error (μs)
1	5.99	±0.06
2	5.92	±0.07
4	4.24	±0.04

Table 6. Luminescence Lifetimes for the Aurophilic $Tb_xGd_{1-x}[Au(CN)_2]_3{\cdot}3H_2O$ Crystals with Terbium Dopant; Lifetimes Were Observed at 541 nm

Tb dopant level (%)	τ_1 (μs)	error (μs)
1	3.95	±0.01
2	3.83	±0.03
4	3.63	±0.02

Tables 7 and 8 below respectively highlight the difference between non-aurophilic and aurophilic frameworks for europium. As with the Tb-doped systems, given the same dopant level, the lifetimes are shorter for the aurophilic samples, for the same reason.

Table 7. Luminescence Lifetimes for the Non-aurophilic $[^nBu_4N]_2[Eu_xGd_{1-x}(NO_3)_4Au(CN)_2]$ Crystals with Europium Dopant; Lifetimes Were Observed at 590 nm

Eu dopant level (%)	τ_1 (μs)	error(μs)
1	4.27	±0.02
2	4.32	±0.05
4	4.52	±0.03
8	4.54	±0.05

Luminescence lifetimes were measured with an oscilloscope for the non-aurophilic $[^nBu_4N]_2[Eu_xTb_{1-x}(NO_3)_4Au(CN)_2]$ and aurophilic $Eu_xTb_{1-x}[Au(CN)_2]_3{\cdot}3H_2O$ systems (Tables S1 and S2 in the SI). Once again, given the same dopant level, the lifetimes are shorter for the aurophilic samples than the non-

dx.doi.org/10.1021/ic500890r | Inorg. Chem. 2014, 53, 7571−7579

Table 8. Luminescence Lifetimes for the Aurophilic $Eu_xGd_{1-x}[Au(CN)_2]_3 \cdot 3H_2O$ Crystals with Europium Dopant; Lifetimes Were Observed at 590 nm

Eu dopant level (%)	τ_1 (μs)	error(μs)
1	4.4	±0.03
2	4.39	±0.03
4	4.3	±0.06
8	4.23	±0.04

aurophilic cases. In all cases the lower the terbium to europium ratio the longer the lifetime, since energy transfer between the dicyanoaurate and Tb^{3+} is being quenched by the Eu^{3+}.

Lifetime measurements were made of the $Eu_xTb_{1-x}[Au(CN)_2]_3 \cdot 3D_2O$ systems (Table S3 in the SI). The H_2O samples had longer lifetimes than their D_2O counterparts. The O−H vibrational energy from the H_2O samples quenches the Ln signal enough to decrease the energy transfer and thereby induce a longer luminescence lifetime. Once again, the lower the ratio between terbium and europium, the longer the luminescence lifetime.

The luminescence and lifetime measurements indicate that energy transfer is possible in aurophilic frameworks but not the non-aurophilic ones. This difference is supported by differences in the crystal structures of the different frameworks. The $^nBu_4N$ cations in the non-aurophilic systems prevent Au−Au interactions that could permit energy transfer between metals and lanthanides. The lack of the $^nBu_4N$ cations in the aurophilic samples allows for Au−Au chain interactions which in turn facilitate efficient energy transfer from the metal centers to the lanthanides and between the lanthanides.

CONCLUSION

The metallophilicity of the framework within aurophilic and non-aurophilic compounds dictates how light interacts with lanthanide ions such as Eu^{3+} and Tb^{3+}. The non-aurophilic frameworks display luminescence for each individual lanthanide ion. In contrast, the aurophilic frameworks allow for energy transfer from the dicyanoaurate donor ion to the lanthanide acceptor ions as the luminescence spectra show. Direct excitation of lanthanide ions in non-aurophilic frameworks is distinguished from Au-Ln^{3+} energy transfer in aurophilic frameworks by examining differences in the excitation spectra. An aurophilic framework allows for efficient energy transfer and therefore shorter luminescence lifetimes. The O−H from the H_2O samples quenches the Ln signal enough to produce a longer luminescence lifetime versus samples with D_2O. Once again, quenching reduces the number of possible pathways for luminescence to occur, thereby decreasing $k_{radiative}$ enough to increase the lifetimes.

In summary, the close proximity of gold(I) centers on neighboring chains in aurophilic frameworks allows for Au−Au interactions to take place that facilitate energy transfer between lanthanides. These Au−Au interactions allow for an overlap between the excitation energy of a lanthanide and the emission energy of the gold or other lanthanide. Conversely, the $^nBu_4N$ ligands in the non-aurophilic systems separate the Au−Au chains preventing aurophilic interactions, thereby limiting the possibility of energy transfer. Further investigation into both types of frameworks with different combinations of lanthanides should yield useful applications for these types of complexes.

ASSOCIATED CONTENT

Supporting Information

X-ray powder diffractograms, luminescence, lifetime, and crystallographic information in CIF format. This material is available free of charge via the Internet at http://pubs.acs.org.

AUTHOR INFORMATION

Corresponding Authors

*E-mail: dleznoff@sfu.ca

*E-mail: howardp@maine.edu

Notes

The authors declare no competing financial interest.

ACKNOWLEDGMENTS

D.B.L. is grateful to NSERC of Canada and R.J.R. to Natural Resources Canada for support of this research. H.H.P. thanks the National Science Foundation for their support in this research (award: CHE-0315877). J.C.A., P.F. and J.M. and H.H.P. are grateful to David Labrecque of the University of Maine for all his assistance in this research.

REFERENCES

(1) Marchal, C.; Filinchuk, Y.; Chen, X.-Y.; Imbert, D.; Mazzanti, M. *Chem.—Eur. J.* **2009**, *15*, 5273−5288.

(2) Eliseeva, S. V.; Bünzli, J.-C. G. *Chem. Soc. Rev.* **2010**, *39*, 189−227.

(3) Carlos, L. D.; Ferreira, R. A. S.; de Zea Bermudez, V.; Ribeiro, S. J. L. *Adv. Mater.* **2009**, *21*, 509−534.

(4) Auzel, F. *Chem. Rev.* **2004**, *104*, 139−73.

(5) Zhong, Y.; Zeng, F.; Chen, J.; Wu, S.; Hou, C.; Tong, Z. *J. Inorg. Organomet. Polym.* **2007**, *17*, 679−685.

(6) Colis, J. C. F.; Staples, R.; Tripp, C.; Labrecque, D.; Patterson, H. *J. Phys. Chem. B* **2005**, *109*, 102−109.

(7) Lu, H.; Yson, R.; Ford, J.; Tracy, H. J.; Carrier, A. B.; Keller, A.; Mullin, J. L.; Poissan, M. J.; Sawan, S.; Patterson, H. H. *Chem. Phys. Lett.* **2007**, *443*, 55−60.

(8) Zang, F. X.; Hong, Z. R.; Li, W. L.; Li, M. T.; Sun, X. Y. *Appl. Phys. Lett.* **2004**, *84*, 2679.

(9) Zang, F. X.; Li, W. L.; Hong, Z. R.; Wei, H. Z.; Li, M. T.; Sun, X. Y.; Lee, C. S. *Appl. Phys. Lett.* **2004**, *84*, 5115.

(10) Poole, R. A; Montgomery, C. P.; New, E. J.; Congreve, A.; Parker, D.; Botta, M. *Org. Biomol. Chem.* **2007**, *5*, 2055−2062.

(11) Okada, K.; Wang, Y.-f.; Nakaya, T.; Inoue, H. *J. Mater. Chem.* **1999**, 3023−3026.

(12) Hidvegi, I.; Gliemann, G. *J. Chem. Phys.* **1982**, *76*, 4361.

(13) Haldar, K. K.; Patra, A. *Appl. Phys. Lett.* **2009**, *95*, 063103.

(14) Atkins, P.; Friedman, R. *Molecular Quantum Mechanics*; 5th ed.; Oxford University Press: New York, 2010.

(15) Roberts, R. J.; Li, X.; Lacey, T. F.; Pan, Z.; Patterson, H. H.; Leznoff, D. B. *Dalton Trans.* **2012**, *41*, 6992−6997.

(16) Cramer, R. E.; Smith, D. W.; Vandoorne, W. *Inorg. Chem.* **1998**, *37*, 5895−5901.

(17) Rawashdeh-omary, M. A.; Omary, M. A.; Patterson, H. H.; May, R. *J. Am. Chem. Soc.* **2000**, *122*, 10371−10380.

(18) Ma, Y.; Che, C.-m; Chao, H.-y. *Adv. Mater.* **1999**, 852−857.

(19) Mansour, M. A.; Connick, W. B.; Lachicotte, R. J.; Gysling, H. J.; Eisenberg, R. *J. Am. Chem. Soc.* **1998**, *120*, 1329−1330.

(20) Katz, M. J.; Ramnial, T.; Yu, H.-Z.; Leznoff, D. B. *J. Am. Chem. Soc.* **2008**, *130*, 10662−10673.

(21) Rocha, J.; Carlos, L. D.; Almeida Paz, F. a.; Ananias, D. *Chem. Soc. Rev.* **2011**, *40*, 926−940.

(22) Cunha-Silva, L.; Lima, S.; Ananias, D.; Silva, P.; Mafra, L.; Carlos, L. D.; Pillinger, M.; Valente, A. a.; Almeida Paz, F. a.; Rocha, J. *J. Mater. Chem.* **2009**, *19*, 2618.

(23) Wang, Y.-F.; Liu, G.-Y.; Sun, L.-D.; Xiao, J.-W.; Zhou, J.-C.; Yan, C.-H. *ACS Nano* **2013**, *7*, 7200−6.

(24) Ong, L. C.; Gnanasammandhan, M. K.; Nagarajan, S.; Zhang, Y. *Luminescence* **2010**, *25*, 290−293.
(25) Auzel, F.; Pecile, D.; Morin, D. *J. Electrochem. Soc.* **1975**, *122*, 101−107.
(26) Assefa, Z.; Patterson, H. H. *Inorg. Chem.* **1994**, *33*, 6194−6200.
(27) Stier, A.; Range, K. *Z. Naturforsch. B* **1996**, *51b*, 698−702.
(28) Stier, A.; Range, K. J. *Z. Kristallogr.* **1997**, *212*, 51.
(29) Yersin, H.; Trümbach, D.; Strasser, J.; Patterson, H. H.; Assefa, Z. *Inorg. Chem.* **1998**, *37*, 3209−3216.
(30) Rawashdeh-omary, M. A.; Larochelle, C. L.; Patterson, H. H. *Inorg. Chem.* **2000**, *39*, 4527−4534.
(31) Colis, J. C. F.; Larochelle, C.; Fernández, E. J.; López-de-Luzuriaga, J. M.; Monge, M.; Laguna, A.; Tripp, C.; Patterson, H. *J. Phys. Chem. B* **2005**, *109*, 4317−4323.
(32) Tanner, P. A; Zhou, X.; Wong, W.-T.; Kratzer, C.; Yersin, H. *J. Phys. Chem. B* **2005**, *109*, 13083−13090.
(33) Larochelle, C. L.; Patterson, H. H. *Chem. Phys. Lett.* **2006**, *429*, 440−444.
(34) Kalachnikova, K.; Assefa, Z.; Sykora, R. E. *Acta Crystallogr.* **2007**, *63*, i162−i162.
(35) Assefa, Z.; Kalachnikova, K.; Haire, R. G.; Sykora, R. E. *J. Solid State Chem.* **2007**, *180*, 3121−3129.
(36) Larochelle, C. L.; Krebs, J. K. *Opt. Mater.* **2008**, *30*, 1446−1450.
(37) Assefa, Z.; Haire, R. G.; Sykora, R. E. *J. Solid State Chem.* **2008**, *181*, 382−391.
(38) Larochelle, C. L.; Seemuller, T. A. *J. Lumin.* **2008**, *128*, 250−256.
(39) Guo, Z.; Yson, R. L.; Patterson, H. H. *Chem. Phys. Lett.* **2007**, *433*, 373−378.
(40) Rodrigues, M. O.; Dutra, J. D. L.; Nunes, L. A. O.; de Sá, G. F.; de Azevedo, W. M.; Silva, P.; Almeida Paz, F. A.; Freire, R. O.; Junior, S. A. *J. Phys. Chem. C* **2012**, *116*, 19951−19957.
(41) Betteridge, P. W.; Carruthers, J. R.; Richard, I.; Prout, K.; Watkin, D. J. *J. Appl. Crystallogr.* **2003**, *36*, 1487.
(42) Barnes, C. L. *J. Appl. Crystallogr.* **1997**, *30*, 568−568.
(43) Fenn, T. D.; Ringe, D.; Petsko, G. A. *J. Appl. Crystallogr.* **2003**, *36*, 944−947.
(44) Baril-Robert, F.; Guo, Z.; Patterson, H. H. *Chem. Phys. Lett.* **2009**, *471*, 258−263.
(45) Kang, C. C.; Liu, R. S. *J. Lumin.* **2007**, *122*−*123*, 574−576.
(46) Kang, J.-G.; Kim, T.-J. *Bull. Korean Chem. Soc.* **2005**, *26*, 1057−1064.
(47) Assefa, Z.; Shankle, G.; Patterson, H. H.; Reynolds, R. *Inorg. Chem.* **1994**, *33*, 2187−2195.
(48) Monguzzi, A.; Milani, A.; Lodi, L.; Trioni, M. I.; Tubino, R.; Castiglioni, C. *New J. Chem.* **2009**, *33*, 1542.